A new model for silicification of cyanobacteria in Proterozoic tidal flats

A new model for silicification of cyanobacteria in Proterozoic tidal flats

Kelsey R. Moore[1]*
Jian Gong[1]
Mihkel Pajusalu[1,2]
Emilie J. Skoog[1]
Megan Xu[1]
Tania Feliz Soto[3]
Victor Sojo[4,5]
Thomas Matreux[5]
Matthew J. Baldes[1]
Dieter Braun[5]
Kenneth Williford[6]
Tanja Bosak[1]

[1] *Department of Earth, Atmospheric and Planetary Sciences, Massachusetts Institute of Technology, Cambridge, MA 02139*
[2] *Tartu Observatory, University of Tartu, Tõravere, Estonia 61602*
[3] *Department of Geology, Bryn Mawr College, Bryn Mawr, PA 19010*
[4] *American Museum of Natural History, New York, NY 10024*
[5] *Department of Physics, Ludwig Maximilian University, München, Germany*
[6] *Jet Propulsion Laboratory, California Institute ofTechnology, Pasadena, CA 91109*

*Corresponding author
Kelsey Moore
Department of Earth, Atmospheric and Planetary Sciences
Massachusetts Institute of Technology
Cambridge, MA 02139
Kelsey.r.moore@jpl.nasa.gov

This is the author manuscript accepted for publication and has undergone full peer review but has not been through the copyediting, typesetting, pagination and proofreading process, which may lead to differences between this version and the Version of Record. Please cite this article as doi: 10.1111/GBI.12447

509-747-7861

Keywords: silicification, cyanobacteria, magnesium, exopolymeric substances (EPS), Proterozoic

1 Acknowledgements

We thank the Simons Foundation for funding this work through grants to T.B. (#327126 and #344707) and JPL for financial support through a Strategic University Research Partnerships (SURP) grant to T.B. and K.W. K.W. acknowledges support of a grant from the National Aeronautics and Space Administration for his work at the Jet Propulsion Laboratory, California Institute of Technology. The research was carried out, in part, at the Jet Propulsion Laboratory, California Institute of Technology, under a contract with the National Aeronautics and Space Administration (80NM0018D0004). This work was done as a private venture and not in the author's capacity as an employee of the Jet Propulsion Laboratory, California Institute of Technology. Samples were collected from Shark Bay, Australia, under a Regulation 17 License, license number 08-000373-1. We thank Dave Holley and the Fenney family for sampling support and Yunbin Guan and Arthur McClelland for support and assistance with sample analysis. We also thank Kurt Konhauser and two anonymous reviewers for helpful comments and suggestions.

DR. KELSEY REED MOORE (Orcid ID : 0000-0001-7332-4098)
DR. JIAN GONG (Orcid ID : 0000-0001-7214-1628)
DR. TANJA BOSAK (Orcid ID : 0000-0001-5179-5323)

Article type : Original Article

A new model for silicification of cyanobacteria in Proterozoic tidal flats

Kelsey R. Moore[1,6]*, Jian Gong[1], Mihkel Pajusalu[1,2], Emilie J. Skoog[1], Megan Xu[1], Tania Feliz Soto[3], Victor Sojo[4,5], Thomas Matreux[5], Matthew J. Baldes[1], Dieter Braun[5], Kenneth Williford[6], Tanja Bosak[1]

[1] Department of Earth, Atmospheric and Planetary Sciences, Massachusetts Institute of Technology, Cambridge, MA 02139
[2] Tartu Observatory, University of Tartu, Tõravere, Estonia 61602
[3] Department of Geology, Bryn Mawr College, Bryn Mawr, PA 19010
[4] American Museum of Natural History, New York, NY 10024
[5] Department of Physics, Ludwig Maximilian University, München, Germany
[6] Jet Propulsion Laboratory, Pasadena, CA 91109

Abstract

Microbial fossils preserved by early diagenetic chert provide a window into the Proterozoic biosphere, but seawater chemistry, microbial processes, and the interactions between microbes and the environment that contributed to this preservation are not well constrained. Here, we use fossilization experiments to explore the processes that preserve marine cyanobacterial biofilms by the precipitation of amorphous silica in seawater medium that is analogous to Proterozoic seawater. These experiments demonstrate that the exceptional silicification of benthic marine cyanobacteria analogous to the oldest diagnostic cyanobacterial fossils requires interactions

among extracellular polymeric substances (EPS), photosynthetically induced pH changes, magnesium cations (Mg^{2+}), and >70 ppm silica.

1 Introduction

Exceptionally preserved Proterozoic fossils are found in lenses and nodules of early diagenetic chert that formed in tidal environments (Sergeev et al., 2012; Butterfield, 2015). These fossiliferous cherts are localized within larger carbonate strata, suggesting that abiotic silica precipitation was not widespread in these environments and that seawater in tidal environments was not saturated with respect to silica. Most estimates suggest values of ~60 ppm silica or less (Siever, 1992; Maliva et al., 2005; Knoll, 2008; Conley et al., 2017), concentrations that are elevated compared to modern seawater but below amorphous silica saturation (120 ppm; Iler, 1979). The localized nature of Proterozoic early diagenetic chert implies that the conditions that led to silica precipitation were met sporadically and points to a microbial role in this silica precipitation (Moore et al., 2020). However, the mechanism behind the preservation of Proterozoic fossils in early diagenetic chert has remained unclear.

Many models of microbial silicification require solutions that are saturated with respect to amorphous silica. Today, this process occurs primarily in hot springs (e.g., Konhauser et al., 2001; Toporski et al., 2002; Yee et al., 2003; Jones et al., 2004; Schultze-Lam et al., 2011) where rapid abiotic precipitation of silica creates sinter deposits that can encase microbes. However, these silica deposits differ from Proterozoic marine tidal flats in both type and scale (Knoll, 2008). Without an appropriate model for Proterozoic-style silicification, we are left to wonder how microbes were silicified in tidal environments, whether dissolved silica concentrations exceeded silica saturation, and how microbial activity or biochemical compounds may have contributed to early silicification and preservation. Recently, we demonstrated the ability of modern coccoidal, benthic cyanobacteria from the hypersaline tidal flats of Shark Bay, Australia, (SBC) to mediate the precipitation of magnesium-rich amorphous silica. This silica preserves the shapes of cells and biofilms in seawater that is undersaturated with respect to silica (Moore et al., 2020), but the specific mechanisms behind this process remained only hypothesized.

Here, we use experimental silicification to test the contributions of different biological and chemical factors to the microbially mediated precipitation of amorphous silica. We compare the silicification potentials of two biochemically distinct cyanobacterial biofilms and

demonstrate that some types of EPS bind silica more readily than others. The precipitation of cell-preserving amorphous silica requires Mg^{2+} and elevated pH driven by photosynthetic activity. The results of this work extend our understanding of the chemical conditions, environmental stresses and microbe-mineral interactions in Proterozoic tidal environments and potential taphonomic biases in the fossil record. Additionally, these results point to magnesium-enriched silica deposits and assemblages of magnesium-silicates and magnesium-carbonates as potential targets for analyses for biosignatures by the upcoming Mars 2020 mission.

2 Methods

2.1 Organism selection and culturing

Two types of cyanobacterial biofilms were used in this study; a previously described enrichment of coccoidal, benthic, pustular mat forming cyanobacteria from Shark Bay, Western Australia (Moore et al., 2020) and Chroococcidiopsis cubana strain CCALA 043 ordered from CCALA (Culture Collections of Autotrophic Organisms, Institute of Botany, Trebon, Czech Republic). Enrichment cultures of Shark Bay cyanobacteria (SBC) were chosen because they have previously been shown to promote silicification in seawater that is undersaturated with respect to silica (Moore et al., 2020). C. cubana was chosen because it is morphologically similar to SBC, but belongs to a different clade in the cyanobacterial tree. We hypothesized based on this distant relationship that it would produce chemically different EPS compared to that of SBC. Enrichment cultures of SBC were grown in modified BG11 medium (Goh et al., 2009; Moore et al., 2020; Supp. Table 4) in sterile plastic plant culture jars (BioExpress, catalog #C-3122-1, 190 mL, 68 mm x 68 mm) at room temperature. Prior to experiments, inoculum cultures were grown and maintained in the presence of continuous light to maximize growth and the culture medium was replaced twice per week to maintain a pH of between 7.5 and 8.5. Pure cultures of C. cubana were maintained in BG11 freshwater medium in sterile plastic culture jars at room temperature with a 12 hr light/12 hr dark cycle and medium was also replaced twice per week. Chroococcidiopsis cubana CCALA 043 genome was previously uploaded to the Joint Genome Institute Integrated Microbial Genomes (JGI IMG; Moore et al., 2019) database and annotated using the IMG Annotation Pipeline v.4.16.5 (Markowitz et al., 2008; Huntemann et al., 2015). Genomes for SBC were sequenced at the MIT BioMicro Center Core Facility, assembled with Megahit v1.0.2, and binned using MetaBAT v2.12.1 (Kang et al., 2015; Li et al., 2015).

Resulting SBC metagenome-assembled genomes (MAGs) were annotated using the same annotation pipeline (Fournier et al., in review, see supplemental methods for the detailed description of the genomic assembly).

2.2 Fossilization experiments

Experimental silicification of biofilms and extracted EPS was carried out in sterile plastic culture jars. Experiments with extracted EPS were conducted in either artificial seawater medium (ASW) or BG11 medium with 90 ppm SiO_2 (sodium silicate solution, Sigma Aldrich SKU#338443; Supp. Table 1 and 2). Experiments on biofilms were conducted only in ASW with 90 ppm silica. Shark Bay cyanobacteria (SBC) or Chroococcidiopsis cubana were inoculated into 80 mL medium and incubated for 15 days at ~21° C with a 12 hour light/12 hour dark cycle. At each time point, fresh biofilms were transferred into 1.5 mL Eppendorf® microtubes (Eppendorf North America, NY, USA, cat#022364111) and gently spun down using a MicroCL 17 Microcentrifuge (ThermoFisher Scientific, NY, USA, cat#75002451) at 4,000 RPM for 10 seconds to remove the liquid and avoid precipitation of minerals and salts. Biofilms pelleted in this manner were immediately fixed in 2.5% glutaraldehyde in 0.1 M sodium cacodylate buffer with 0.1% $CaCl_2$ at pH 7.4 at 4° C overnight. Ten mL of medium were removed and replaced at each sampling point to replenish nutrients and silica. A separate set of biofilms sampled on day 15 were collected, rinsed with milliQ water, and mounted onto silicon wafers for NanoSIMS analysis.

The silicification of extracted EPS (see supplemental methods for extraction procedures), was assessed by adding EPS directly to 50 mL of sterile medium (either ASW, BG11, or ASW that lacked Mg^{2+}, all with 90 ppm silica) and incubating the solution for two days at ~21° C. One mL samples of media were collected and filtered using 0.05 µm polycarbonate filters into sterile 1.5 mL Eppendorf® microtubes. Titration experiments following Braissant et al. (2007) were used to determine the pKa of EPS extracts. The concentration of dissolved silica was measured using the molybdate blue spectrophotometry method (Strickland & Parsons, 1972). Supplemental methods provide additional details related to the titration of EPS and silica assay procedure.

2.3 Microscopy

To prepare samples for scanning electron microscopy (SEM) and Energy Dispersive X-Ray Spectroscopy (EDS), fixed biofilm samples were washed in a 0.2 mM sodium cacodylate buffer, rinsed four times with milliQ water ≥18.2 MΩ x cm and dried using an ethanol dehydration series (50%, 80%, 90% and 100% ethanol in 10 minute steps). Once dry, samples were mounted with double-coated carbon conductive tape (Ted Pella Inc., Product #16084-7, Redding, CA, USA) onto 12.7 mm diameter SEM stubs (Ted Pella Inc., Product #16111, Redding, CA, USA). Mounted dried samples were coated with an 80:20 mixture of Pt:Pd using a HAR-052 Carbon Coater equipped with a metal coater and imaged and analyzed with a JEOL 7900F SEM at the Harvard Center for Nanoscale Systems (CNS). Images were collected at 3 keV accelerating voltage. For chemical analysis, total area EDS spectra were collected in at least three regions per biofilm at 10 keV and processed using AZtec software (Oxford Instruments, Abingdon, United Kingdom).

2.4 NanoSIMS

Biofilm samples that grew in ASW with 90 ppm silica for 15 days were prepared for NanoSIMS as follows: samples were rinsed with milliQ water ≥18.2 MΩ x cm, placed onto 1 inch silicon wafers (Ted Pella Inc., Redding, CA, USA, catalog #16011) and left to air dry overnight in a biosafety hood. Samples were coated with gold on a HR Metal Sputtering Coater at the Caltech GPS Division Analytical Facility and analyzed by the Cameca NanoSIMS 50L at the Caltech Microanalysis Center with a Cs^+ ion beam. For each sample, a 20 µm - 25 µm raster was pre-sputtered using a beam current of 1 nA for approximately 2 minutes. Both ion maps and ion count data were collected using a beam current of 2 pA and the ^{28}Si detector on a minimum of two regions per biofilm for 15 minutes. Data were analyzed using L'image software (Larry Nittler, Carnegie Institute of Washington) and total ^{28}Si counts were calculated for identically sized regions of each biofilm (12 µm x 12 µm).

2.5 FT-IR

Fourier-Transform Infrared Spectroscopy (FT-IR) was used to characterize the composition of extracted EPS and to analyze silica in the extracted EPS. After the precipitation of raw EPS extracts with ethanol at 4° C, an aliquot of the precipitated material was transferred to a 1.5 mL Eppendorf® microtubes and centrifuged. The supernatant was removed and the

samples were left to dry overnight in a biosafety hood. For silicified EPS, the liquid media were vacuum-filtered through 0.2 µm Isopore Membrane Filter (Millipore Sigma, Billerica, MA, USA, catalog # GTTP04700). Raw extracts, filtered extracts from experiments, and filter paper controls were analyzed using the Bruker FT-IR microscope in the Center for Nanoscale Systems (Harvard University). A minimum of six spots per sample was analyzed and spectra were processed using Opus Spectroscopy Software.

3 Results:

3.1 Biological contribution to silicification

Biofilms made by coccoidal, benthic, marine cyanobacteria from Shark Bay (SBC) mediate the precipitation of magnesium-rich amorphous silica (Moore et al., 2020). Because silica precipitates are always observed in association with the EPS that coats and connects cells, we hypothesized that EPS was the site of silica nucleation. To confirm this, we added 14 mg of EPS extracted from SBC to duplicate sterile plastic culture jars that contained ASW with 90 ppm silica at pH 8. These extracts are chemically complex, but contain abundant polysaccharides, as demonstrated by assays that measured twice as many carbohydrate components per unit volume of dissolved EPS compared to protein (0.06 g/L versus 0.03 g/L). Dissolved silica concentrations decreased by 13 +/- 3% after 2 days in jars that contained SBC EPS but did not decrease within error in sterile controls. Thus, even in the absence of cellular activity, EPS produced by SBC mediated the precipitation of silica from seawater that is undersaturated with respect to amorphous silica.

To assess the universality of this microbially mediated silica precipitation and the fossilization potential of other benthic cyanobacteria, we compared the silicification of SBC to that of Chroococcidiopsis cubana. C. cubana is a coccoidal, benthic, mat-forming cyanobacterium that is morphologically similar to SBC, but belongs to a distinct clade (Supp. Fig 1). EDS spectra of SBC biofilms showed higher intensity sulfur peaks than those of C. cubana biofilms, indicating that the two types of cyanobacteria had chemically distinct EPS (Fig. 1). Consistent with this difference in biofilm-associated sulfur, FT-IR spectra of EPS extracted from SBC contained prominent peaks at 1250 cm^{-1}, 1370 cm^{-1}, 840 cm^{-1}, 830 cm^{-1} and 805 cm^{-1} in SBC EPS, indicative of sulfate esters and sulfated galactose units (Rodriguez-Jasso et al., 2011; Souza et al., 2012; Fig. 1). Titration of EPS extracted from SBC biofilms showed that it

contained functional groups with pKa 2.89, 6.20, 7.67, and 8.87 (Supp. Fig. 2), as expected from sulfur-containing surface groups with pKa values between 7 and 10 (Braissant et al., 2007). In contrast, FT-IR spectra of EPS extracted from C. cubana did not contain peaks indicative of sulfated polysaccharides (Fig. 1) and the titration of their EPS showed that it only contained functional groups with pKa of 6.2 or less (Supp. Fig. 2). Indeed, genes responsible for the production of sulfated polysaccharides in the SBC genomes, but not in the genome of C. cubana, an organism isolated from a sulfate-poor environment (see supplemental methods for further details). These combined analyses revealed that, although both organisms are morphologically similar cyanobacteria, they produced chemically distinct EPS.

To test whether or not both types of cyanobacteria and cyanobacterial EPS could promote the precipitation of amorphous silica and mediate preservation, we incubated biofilms made by SBC and C. cubana in batch cultures in sterile plastic culture jars that contained ASW with 90 ppm silica. All batch culture experiments were conducted in duplicate and included sterile controls to confirm that no abiotic silica precipitation occurred. Both biofilms were viable and grew under our experimental conditions: we measured a 7.8 mg and 12.1 mg increase in biomass of C. cubana and SBC, respectively. After 15 days, colloidal precipitates coated the surfaces of SBC biofilms and magnesium and silicon peaks appeared in the EDS spectra (Fig. 2a). This demonstrated that amorphous, magnesium-rich silica precipitated in the SBC biofilms. In contrast, C. cubana biofilms contained only rare patches of colloidal precipitates and their EDS spectra revealed much lower intensity magnesium and silicon peaks compared to those observed in SBC biofilms (Fig. 2b). To quantify the amount of silica that accumulated in SBC and C. cubana, we mapped two identically sized regions of each biofilm that were incubated under the same conditions for 15 days using NanoSIMS. Total ^{28}Si counts in the ion maps were 2.8 times higher in SBC biofilms compared to the counts in identically sized areas of C. cubana biofilms (Fig. 3), consistent with the SEM/EDS observations. To test whether these chemical differences were associated with different silicification potentials of EPS in the absence of cellular activity, we incubated EPS extracted from C. cubana and SBC in duplicate for 2 days at 20 mg EPS per 80 mL ASW with 90 ppm silica. EPS from C. cubana induced a <3% decrease in silica concentration compared to the 13% decrease in silica concentration induced by SBC EPS. These combined experiments confirmed the stronger potential of the sulfate-rich EPS produced by SBC to precipitate magnesium-rich silica than EPS compared to the EPS produced by C. cubana.

3.2 The role of pH and photosynthetic activity in silicification

In undersaturated solutions, silica coats and preserves cells only when cyanobacterial mats are living and photosynthesizing at the surface (Moore et al., 2020). We hypothesized that this may be related to the increased pH due to photosynthesis and the resulting interactions among organic compounds and the seawater. When SBC biofilms grew with a 12 hour light/12 hour dark cycle, the pH values fluctuated daily due to photosynthetic activity and the average pH increased from 7.7 to more than 8 over 5 days (Supp. Fig. 3). To test the role of photosynthetically driven pH increase on silicification, we incubated SBC biofilms in duplicate in ASW with 90 ppm silica under two pH regimes that were maintained by medium replacement every 5 days (ASW pH<7.5 and pH>7.5; Supp. Fig. 4). Silica did not precipitate after 25 days in sterile ASW controls in either pH condition. Biofilms incubated under both conditions accumulated magnesium-rich silica, but the intensities of silicon and magnesium peaks were higher in the cultures that grew at pH>7.5 and these biofilms were more extensively covered by nanoscopic grainy silica precipitates (Fig. 4). This supported the contribution of elevated pH to the precipitation of amorphous magnesium-rich silica in SBC EPS.

To confirm the role of pH on the silicification of organic surfaces in the absence of cells and cellular metabolisms, we added 14 mg of extracted SBC EPS in duplicate to 50 mL ASW titrated to either pH 6.9 or pH 8.7 with 90 ppm silica for 2 days. The behavior of EPS in biofilms and its interactions with ions in solution depend on the pH of the solution and the pKa of the dominant functional groups in the EPS. When pH<pKa, these functional groups should be mostly protonated, when pH>pKa, they should be mostly deprotonated (Dogsa et al., 2005; Wang et al., 2012). Therefore, when pH>7.76, functional groups in SBC EPS should be predominantly deprotonated and able to interact with ions in solution. Silica concentrations did not decrease measurably in sterile controls without EPS at either pH or within error (<3%) in ASW with EPS at pH 6.9, but we measured a 7 +/- 3% decrease in pH 8.7 ASW. Peaks at 1100 cm^{-1} and at 800 cm^{-1} in the FT-IR spectra of EPS collected from after 2 days confirmed the presence of amorphous silica (Fig. 5; Bertaux et al., 1998). These results show that, by increasing the pH of the solution, photosynthetic activity or any other pH-increasing metabolisms may create microenvironments that favor the accumulation of ions and silica by EPS in modern seawater. Previous modeling, observational and experimental work indicates that

local pH changes induced by photosynthesis in the polymers that surround cells and stimulate mineral precipitation in solutions that contain high concentrations of dissolved inorganic carbon (DIC; Arp et a., 1999; Bosak and Newman, 2003). Thus, combined with the observes microbial binding of silica at pH>7.5, local pH changes around the EPS of photosynthetic biofilms can be expected to promote the precipitation of amorphous, magnesium-rich silica even under Proterozoic-like DIC conditions in seawater that is undersaturated with respect to silica.

3.3 The role of salinity in silicification

The dominant form of dissolved silica in an undersaturated solution at circumneutral pH is deprotonated silicic acid that carries a negative charge ($SiO_4H_3^-$; Iler, 1979). If the negatively charged, deprotonated functional groups such as sulfate in cyanobacterial EPS sequester silica at high pH, a chemical intermediary is required to bridge the negatively charged functional groups and negatively charged silicic acid. Studies of silicification in iron-rich hot springs report a co-increase in iron and silicon in silicified biofilms and suggest that Fe^{3+} acts as a cation bridge between negatively charged cell surfaces and silica in solution (Urrutia & Beveridge, 1994; Konhauser et al., 2004). ASW medium contained only a small amount of iron (<2 µM) and iron was not detected in either the silicified or unsilicified biofilms. Instead, the EDS spectra of colloidal precipitates in SBC biofilms consistently documented high intensity magnesium and silicon peaks. This suggested a role for Mg^{2+} as a bridge between silicic acid and the negatively charged surface groups in the EPS.

To assess the effect of Mg^{2+} on silica accumulation, we measured the change in dissolved silica concentration when 7 mg EPS and 90 ppm silica were added to 25 mL of either freshwater medium (BG11) that contained 0.6 mM Mg^{2+} or ASW that lacked Mg^{2+}. Both media were titrated to an initial pH 7.4. All conditions were tested in duplicate and silica did not precipitate in the absence of EPS under any of the experimental conditions tested. SBC EPS induced a <3% decrease in silica in freshwater medium (BG11) with 90 ppm SiO_2 and in ASW that lacked Mg^{2+}, all compared to the 13 +/- 3% decrease observed in ASW that contained 50 mM Mg^{2+}. Thus, SBC EPS accumulated less silica in the absence of Mg^{2+}.

Past studies have demonstrated a shift toward more positive zeta potentials of organic molecules with increasing salt content and pH (Salgin et al., 2012). This could explain the ability of EPS to sequester negatively charged silicic acid more effectively in seawater with elevated

pH. To assess the impact of salinity on SBC biofilms, we measured their zeta potential in milliQ water and in ASW. SBC biofilms had zeta potential values of -7.6 +/- 2 mV in seawater and a lower zeta potential of -31 +/- 1 mV after transfer from seawater to milliQ water. The concentration of Mg^{2+} in milliQ after this transfer increased by 0.75 mM, confirming the release of bound Mg^{2+} from the biofilms. The shift toward a more positive surface charge of EPS due to the adsorption of Mg^{2+} and other cations from seawater could improve the binding of negatively charged silicic acid in solution by biofilm surfaces and initiate the precipitation of amorphous magnesium-rich silica through cation bridging. Future work that explores microbial silicification in iron-, magnesium- and carbonate-rich environments, such as the past environments in Jezero Crater on Mars (Tarnas et al., 2019; Horgan et al., 2020), should consider the potential contributions of magnesium and other cations in this cation bridging.

4. Discussion

4.1 Silicification of EPS and microbial stress responses

Previous studies have described passive nucleation of silica on EPS in supersaturated solutions and environments where silica already precipitates abiotically (e.g., Konhauser et al., 2001; Yee et al., 2003; Jones et al., 2004; Lalonde et al., 2005; Handley et al., 2008; Schultze-Lam et al., 2011). The results presented here support a stronger role for EPS in silicification and in fact show that magnesium-rich amorphous silica can nucleate on EPS in seawater that is undersaturated with respect to silica. Some previous studies hypothesized that organic compounds contributed to the precipitation of dolomite-sepiolite (Leguey et al., 2010). To our knowledge, this is the first demonstration of such interactions between organic compounds.

The ability of SBC EPS to promote silica precipitation more readily than the EPS produced by C. cubana under identical chemical conditions points to potential taphonomic bias in the record of silicified Proterozoic microbes. Past work has suggested that even in solutions that are saturated with respect to amorphous silica, some organic compounds and functional groups bind silica more readily than others (e.g., Lalonde et al., 2005; Orange et al., 2009). Our results expand these findings to conditions where silica concentrations are below saturation and show that cyanobacterial silicification Proterozoic likely depended not only on the presence of EPS envelopes (Golubic & Seong-Joo, 1999; Sergeev et al., 2012; Butterfield, 2015 and

309 references therein), but also on the chemical composition of EPS produced by different
310 organisms.
311 If, as our results show, some cyanobacteria and EPS bind silica and promote the
312 precipitation of magnesium-rich amorphous silica from undersaturated solutions better than
313 others, these organism- and environment-dependent biochemical differences may have
314 introduced biases in the fossil record. Modern cyanobacteria and algae that colonize hypersaline
315 environments are exposed to stresses such as desiccation, high salinity, and UV radiation and
316 many produce thick envelopes of EPS. Many assemblages of Proterozoic cyanobacteria were
317 silicified in similarly exposed, hypersaline environments (Butterfield 2015), and the organisms
318 that thrived in these environments also produced EPS in response to the same stresses. This EPS
319 is preserved in the rock record, consistent with our findings that microbial EPS is the driving
320 force behind silicification. Sulfated polysaccharides, which seem to particularly benefit
321 organisms exposed to osmotic and other stresses (Costa et al., 2010; Jiao et al., 2011;
322 Raguraman et al., 2019), may have also been produced by Proterozoic cyanobacteria in
323 hypersaline tidal environments with locally elevated sulfate concentrations (e.g., Hodgskiss et
324 al., 2019; Bell and Jackson, 1974). The specific abilities of sulfated polysaccharides and other
325 components of the SBC EPS matrix to bind silica remain to be explored.
326
327 **4.2 Evidence for interactions among cations, EPS and silica in the rock record**
328 By teasing apart the biological and chemical factors that may have facilitated
329 silicification in Proterozoic tidal environments, we can gain a better understanding of chemical
330 conditions and microbe-environment interactions during this eon. The localized nature of
331 fossiliferous early diagenetic chert within carbonate strata from the Proterozoic (e.g., Hofmann,
332 1976; Oehler, 1978; Knoll, 2008) suggests that these environments did not see widespread
333 abiotic precipitation from saturated seawater. Instead, our results highlight the importance of
334 local biological and biochemical factors such as photosynthetically or other metabolically driven
335 pH changes, the composition of EPS, and the interactions of EPS with magnesium and silica in
336 solution for silicification. Together, these biological and abiotic factors may have also
337 contributed to silicification in Proterozoic tidal environments even when silica concentrations
338 were below saturation.

Our results demonstrate that interactions among Mg^{2+}, EPS and silica are instrumental in the biologically mediated silicification of modern marine cyanobacteria. Indeed, magnesium-rich silica phases that nucleate around cyanobacterial cells and organic particles have been reported in modern microbial mats from various localities (Kremer et al., 2008; Pacton et al., 2015; Zeyen et al., 2015; Perri et al., 2018). Already abundant in seawater, Mg^{2+} would have been even more concentrated in supratidal hypersaline environments such as those that preserved many silicified Proterozoic fossils and similar interactions between Mg^{2+} and organic surfaces may have played a role in the preservation of fossils and organic matter during the Proterozoic. If so, we would expect to see magnesium-rich silica in organic-rich fossiliferous dolomite-hosted Proterozoic chert from tidal environments. If not, magnesium should be present only in the dolomite that surrounds chert nodules.

As a proof of this concept, we mapped the distributions of calcium, carbon, magnesium, and silicon by EDS in a thin section of the Balbirini Dolomite (thin section 106A on loan from Geosciences Australia; Oehler, 1978). We selected these samples because the Balbirini Dolomite is a well-documented Proterozoic supratidal deposit that contains fossiliferous chert nodules with exceptionally preserved microbial lamination and cyanobacterial fossils, including Eoentophysalis, the direct morphological analogs of SBC (Oehler, 1978). Chert and dolomite occur in close proximity, both preserve organic-rich laminae, but only chert preserves cyanobacterial body fossils (Oehler, 1978). Petrographic and SEM images confirmed the presence of fossils in chert and the continuity of organic-rich microbial lamination across chert and dolomite (Fig. 6). Silicified regions contained organic carbon and the silicon and calcium maps followed the distinct chert-dolomite boundaries (Fig. 6; region comparable to those illustrated in Fig. 3 in Oehler, 1978). Magnesium was abundant in dolomite, but, unlike calcium, was also present in the organic- and fossil-rich silicified regions (Fig. 6). Some regions that contained high counts of silica and magnesium additionally contained aluminum (Supp. Fig. 5). These observations revealed a spatial association between magnesium and silicon phases in the microbially laminated horizons of the Balbirini Dolomite, consistent with the initial microbially-mediated precipitation of magnesium-rich amorphous silica. The presence of aluminum also points to the potential role of this cation in the formation of chert and other silica phases that nucleate on EPS.

4.3 Sporadic silicification in carbonate-depositing environments

Although the dolomite that surrounds chert lenses in the Balbirini Dolomite does not preserve exquisite body fossils, it does preserve organic-rich microbial laminae. EPS from sulfate reducing bacteria can nucleate and precipitate protodolomite in modern sabkhas (Bontognali et al., 2014) or in seawater (Krause et al., 2012). Anoxygenic phototrophs also promote the precipitation of dolomite that preserves organic textures and microbial lamination in less saline environments (Daye et al., 2019). Thus, the preferential binding of Mg^{2+} from seawater by organic surfaces in complex microbial mats may have contributed to the precipitation of both chert and magnesium-rich carbonate minerals in Proterozoic tidal flats. The chemical conditions, gradients in the EPS composition from the surfaces to the interiors of microbial mats, and the balance between the production and degradation of EPS may have driven the location and timing of chert and carbonate precipitation in the same tidal flat.

Experiments demonstrated the extensive precipitation of magnesium-rich silica in photosynthetically active SBC biofilms at silica concentrations above 70 ppm (Moore et al., 2020). If this was also the case in Proterozoic tidal environments, this could account for the distribution of chert and dolomite in the range of microenvironments. The patchy distribution of nodules and lenses of fossiliferous cherts in supratidal deposits could indicate that photosynthetically active biofilms were only preserved when exposed to seawater that contained 70 ppm silica or more. Subtidal deposits that contain more laterally extensive chert layers may have precipitated when photosynthetically active biofilms experienced sustained exposure to hypersaline water, allowing for prolonged chert precipitation and fossil preservation. In contrast, micritic carbonate minerals in modern peritidal environments precipitate primarily below the photic zone in permanently or frequently anaerobic zones that contain extensively degraded EPS (e.g., Bontognali et al., 2010). Compositional changes in EPS, metabolic gradients and environmental physicochemical gradients that enable the preservation of microbial body fossils in chert and laminae in dolomite remain to be constrained. The interplay between these factors and mineral precipitation could extend our understanding of Proterozoic communities and environmental parameters.

5 Model

Our experimental findings identify the central role of microbial EPS and ions in solution in the silicification of benthic photosynthetic mats. We reveal a novel mechanism that explains the preservation of microbial body fossils, organic matter and mat textures in oxygenated marine environments where silica does not precipitate abiotically (Fig. 7). Magnesium-rich amorphous silica nucleates within the EPS and its precipitation is favored when pH values exceed pKa values of the dominant functional groups in the EPS. Because of this pH dependence, microbial metabolisms that increase the local pH, such as photosynthesis, can promote early silicification. Mg^{2+} plays a key role in silicification, likely by acting as a cation bridge between silicic acid and negatively charged functional groups in the EPS. These findings attribute the formation of early diagenetic chert and fossilization of microbes to interactions among photosynthetically driven pH changes, water chemistry, and the production of EPS in response to environmental stress. This model can account for the localized occurrence of chert nodules and lenses within Proterozoic carbonate deposits, such as the Proterozoic Balbirini Dolomite, and presents a new mechanism to explain silicification and the formation of early diagenetic chert in Proterozoic tidal flats.

6 References

Arp G, Reimer A, Reitner J (1999) Calcification in cyanobacterial biofilms of alkaline salt lakes. European Journal of Phycology **34**, 393-403.

Bell RT, Jackson GD (1974) Aphebian halite and sulphate indications in the Belcher Group, Northwest Territories. Canadian Journal of Earth Sciences **11**, 722-728.

Bertaux J, Froehlich F, Ildefonse P (1998) Multicomponent analysis of FTIR spectra; quantification of amorphous and crystallized mineral phases in synthetic and natural sediments. Journal of Sedimentary Research **68**, 440–447.

Blättler CL, Claire MW, Prave AR, Kirsimäe K, Higgins JA, Medvedev P V., Romashkin AE, Rychanchik D V., Zerkle AL, Paiste K, Kreitsmann T, Millar IL, Hayles JA, Bao H, Turchyn A V., Warke MR, Lepland A (2018) Two-billion-year-old evaporites capture Earth's great oxidation. Science **360**, 320–323.

Bontognali TRR, Mckenzie JA, Warthmann RJ, Vasconcelos C (2014) Microbially influenced formation of Mg-calcite and Ca-dolomite in the presence of exopolymeric substances produced by sulphate-reducing bacteria. Terra Nova **26**, 72–77.

Bosak T, Newman D (2003) Microbial nucleation of calcium carbonate in the Precambrian. Geology **31**, 577-580.

Braissant O, Decho AW, Dupraz C, Glunk C, Visscher PT (2007) Exopolymeric substances of sulfate-reducing bacteria: Interactions with calcium at alkaline pH and implication for formation of carbonate minerals. Geobiology **5**, 401–411.

Butterfield NJ (2015) Proterozoic photosynthesis - a critical review. Palaeontology **58**, 953–972.

Conley DJ, Frings PJ, Fontorbe G, Clymans W (2017) Biosilicification drives a decline of dissolved Si in the oceans through geologic time. Frontiers in Marine Science **4**, 1–19.

Costa LS, Fidelis GP, Cordeiro SL, Oliveira RM, Sabry DA, Câmara RBG, Nobre LTDB, Costa MSSP, Almeida-Lima J, Farias EHC, Leite EL, Rocha HAO (2010) Biological activities of sulfated polysaccharides from tropical seaweeds. Biomedicine and Pharmacotherapy **64**, 21–28.

Daye M, Higgins J, Bosak T (2019) Formation of ordered dolomite in anaerobic photosynthetic biofilms. Geology **47**, 509–512.

Dogsa I, Kriechbaum M, Stopar D, Laggner P (2005) Structure of bacterial extracellular polymeric substances at different pH values as determined by SAXS. Biophysical Journal **89**, 2711–2720.

Goh F, Allen MA, Leuko S, Kawaguchi T, Decho AW, Burns BP, Neilan B a (2009) Determining the specific microbial populations and their spatial distribution within the stromatolite ecosystem of Shark Bay. The ISME journal **3**, 383–396.

Golubic S, Seong-Joo L (1999) Early cyanobacterial fossil record: preservation, palaeoenvironments and identification. European Journal of Phycology **34**, 339–348.

Handley KM, Turner SJ, Campbell KA, Mountain BW (2008) Silicifying biofilm exopolymers on a hot-spring microstromatolite: Templating nanometer-thick laminae. Astrobiology **8**, 747–770.

Hodgskiss MSW, Dagnaud OMJ, Frost JL, Halverson GP, Schmitz MD, Swanson-Hysell NL, Sperling EA (2019) New insights on the Orosirian carbon cycle, early Cyanobacteria, and the assembly of Laurentia from the Paleoproterozoic Belcher Group. Earth and Planetary Science Letters **520**, 141–152.

Hofmann HJ (1976) Precambrian microflora, Belcher Islands, Canada: Significance and systematics. Journal of Paleontology **50**, 1040–1073.

462 Horgan BHN, Anderson RB, Dromart G, Amador ES, Rice MS (2020) The mineral diversity of
463 Jezero crater: Evidence for possible lacustrine carbonates on Mars. Icarus **339**, 113526.
464 Huntemann M, Ivanova NN, Mavromatis K, James Tripp H, Paez-Espino D, Palaniappan K,
465 Szeto E, Pillay M, Chen IMA, Pati A, Nielsen T, Markowitz VM, Kyrpides NC (2015)
466 The standard operating procedure of the DOE-JGI Microbial Genome Annotation
467 Pipeline (MGAP v.4). Standards in Genomic Sciences **10**, 4–9.
468 Iler RK (1979) The chemistry of silica: solubility, polymerization, colloid and surface properties
469 and biochemistry of silica. John Wiley and Sons, New York.
470 Jiao G, Yu G, Zhang J, Ewart HS (2011) Chemical structures and bioactivities of sulfated
471 polysaccharides from marine algae. Marine Drugs **9**, 196–233.
472 Jones B, Konhauser KO, Renaut RW, Wheeler RS (2004) Microbial silicification in Iodine Pool,
473 Waimangu geothermal area, North Island, New Zealand: Implications for recognition and
474 identification of ancient silicified microbes. Journal of the Geological Society **161**, 983–
475 993.
476 Kang DD, Froula J, Egan R, Wang Z (2015) MetaBAT, an efficient tool for accurately
477 reconstructing single genomes from complex microbial communities. PeerJ 1–15.
478 Knoll AH (2008) Cyanobacteria and Earth History. In: The Cyanobacteria: Molecular Biology,
479 Genomics and Evolution (eds. Herrero A, Flores E). Caister Academic Press.
480 Konhauser KO, Jones B, Phoenix VR, Ferris G, Renaut RW (2004) The microbial role in hot
481 spring silicification. Ambio **33**, 552–558.
482 Konhauser KO, Phoenix VR, Bottrell SH, Adams DG, Head IM (2001) Microbial-silica
483 interactions in Icelandic hot spring sinter: Possible analogues for some Precambrian
484 siliceous stromatolites. Sedimentology **48**, 415–433.
485 Krause S, Liebetrau V, Gorb S, Sanchez-Roman M, McKenzie JA, Treude T (2012) Microbial
486 nucleation of Mg-rich dolomite in exopolymeric substances under anoxic modern
487 seawater salinity: New insight into an old enigma. Geology **40**, 587-590.
488 Kremer B, Kazmierczak J, Stal LJ (2008) Calcium carbonate precipitation in cyanobacterial mats
489 from sandy tidal flats of the North Sea. Geobiology **6**, 46–56.
490 Lalonde S V, Konhauser KO, Reysenbach AL, Ferris FG (2005) The experimental silicification
491 of Aquificales and their role in hot spring sinter formation. Geobiology **3**, 41–52.
492 Leguey S, Ruiz De Leon D, Ruiz AI, Cuevas J (2010) The role of biomineralization in the origin

of sepiolite and dolomite. American Journal of Science **310**, 165–193.

Li D, Liu CM, Luo R, Sadakane K, Lam TW (2015) MEGAHIT: An ultra-fast single-node solution for large and complex metagenomics assembly via succinct de Bruijn graph. Bioinformatics **31**, 1674–1676.

Maliva RG, Knoll AH, Simonson BM (2005) Secular change in the Precambrian silica cycle: Insights from chert petrology. GSA Bulletin **117**, 835–845.

Markowitz VM, Szeto E, Palaniappan K, Grechkin Y, Chu K, Chen IMA, Dubchak I, Anderson I, Lykidis A, Mavromatis K, Ivanova NN, Kyrpides NC (2008) The integrated microbial genomes (IMG) system in 2007: Data content and analysis tool extensions. Nucleic Acids Research **36**, 528–533.

Moore KR, Magnabosco C, Momper L, Gold DA, Bosak T, Fournier GP (2019) An expanded ribosomal phylogeny of cyanobacteria supports a deep placement of plastids. Frontiers in Microbiology **10**, 1–14.

Moore KR, Pajusalu M, Gong J, Sojo V, Matreux T, Braun D, Bosak T (2020) Biologically mediated silicification of marine cyanobacteria and implications for the Proterozoic fossil record. Geology 1–5.

Oehler DZ (1978) Microflora of the middle Proterozoic Balbirini Dolomite (McArthur Group) of Australia. Alcheringa **2**, 269–307.

Orange F, Westall F, Disnar JR, Prieur D, Bienvenu N, Romancer M Le, Defarge C (2009) Experimental silicification of the extremophilic Archaea Pyrococcus abyssi and Methanocaldococcus jannaschii: applications in the search for evidence of life in early Earth and extraterrestrial rocks. Geobiology **7**, 403–418.

Pacton M, Sorrel P, Bevillard B, Zacai A, Vincon-Laugier A, Oberjansli H (2015) Sedimentary facies analyses from nano- to millimetre scale exploring past microbial activity in a high-altitude lake (Lake Son Kul , Central Asia). Geology Magazine **152**, 902–922.

Perri E, Tucker ME, Slowakiewcz M, Whitaker F, Bowen L, Perrotta ID (2018) Carbonate and silicate biomineralization in a hypersaline microbial mat (Mesaieed sabkha , Qatar): Roles of bacteria, extracellular polymeric substances and viruses. Sedimentology **65**, 1213–1245.

Raguraman V, Abraham L S, Jyotsna J, Palaniappan S, Gopal S, Thirugnanasambandam R, Kirubagaran R (2019) Sulfated polysaccharide from Sargassum tenerrimum attenuates

oxidative stress induced reactive oxygen species production in in vitro and in zebrafish model. Carbohydrate Polymers **203**, 441–449.

Rodriguez-Jasso RM, Mussatto SI, Pastrana L, Aguilar CN, Teixeira JA (2011) Microwave-assisted extraction of sulfated polysaccharides (fucoidan) from brown seaweed. Carbohydrate Polymers **86**, 1137–1144.

Salgin S, Salgin U, Bahadir S (2012) Zeta potentials and isoelectric points of biomolecules: The effects of ion types and ionic strengths. International Journal of Electrochemical Science **7**, 12404–12414.

Schultze-Lam S, Ferris FG, Konhauser KO, Wiese RG (2011) In situ silicification of an Icelandic hot spring microbial mat: Implications for microfossil formation. Canadian Journal of Earth Sciences **32**, 2021–2026.

Sergeev VN, Sharma M, Shukla Y (2012) Proterozoic Fossil Cyanobacteria. The Palaeobotanist **61**, 189–358.

Siever R (1992) The silica cycle in the Precambrian. Geochimica et Cosmochimica Acta **56**, 3265–3272.

Souza BWS, Cerqueira MA, Bourbon AI, Pinheiro AC, Martins JT, Teixeira JA, Coimbra MA, Vicente AA (2012) Chemical characterization and antioxidant activity of sulfated polysaccharide from the red seaweed Gracilaria birdiae. Food Hydrocolloids **27**, 287–292.

Strickland JDH, Parsons TR (1972) Determination of reactive silicate. In: A Practical Handbook of Seawater Analysis: Fisheries Research Board of Canada. pp. 65–70.

Tarnas JD, Mustard JF, Lin H, Goudge TA, Amador ES, Bramble MS, Kremer CH, Zhang X, Itoh Y, Parente M (2019) Orbital identification of hydrated silica in Jezero Crater, Mars. Geophysical Research Letters **46**, 12771–12782.

Urrutia MM, Beveridge TJ (1994) Formation of fine-grained silicate minerals and metal precipitates by a bacterial surface (Bacillus subtilis). Chemical Geology **116**, 261–280.

Wang L-L, Wang L-F, Ren X-M, Ye X-D, Li W-W, Yuan S-J, Sun M, Sheng G-P, Yu H-Q, Wang X-K (2012) pH dependence of structure and surface properties of microbial EPS. Environmental Science and Technology **46**, 737–744.

Yee N, Phoenix VR, Konhauser KO, Benning LG, Ferris FG (2003) The effect of cyanobacteria on silica precipitation at neutral pH: Implications for bacterial silicification in geothermal

hot springs. Chemical Geology **199**, 83–90.

Zeyen N, Benzerara K, Li J, Groleau A, Balan E, Robert J, Estève I, Tavera R, Moreira D, López-García P (2015) Formation of low-T hydrated silicates in modern microbialites from Mexico and implications for microbial fossilization. Frontiers in Earth Science **3**, 1–23.

Figure captions:

Fig. 1: SEM images and EDS spectra of SBC and C. cubana biofilms show that SBC biofilms contain more sulfur compared to those of C. cubana. FT-IR spectra of extracted SBC EPS and C. cubana EPS. Spectra show similar bond vibrations and EPS composition from these cultures, but the SBC EPS spectrum contains additional peaks indicative of sulfate groups which are not present in the EPS from C. cubana.

Fig. 2: Representative SEM images and corresponding EDS spectra of SBC and C. cubana biofilms after 15 days of fossilization experiments. Colloidal precipitates are common in SBC biofilms and rare in C. cubana biofilms. The EDS spectrum of SBC biofilms contains a higher intensity silicon peak compared to that of C. cubana. SBC biofilms contain magnesium and sulfur, these elements are much less abundant in C. cubana biofilms.

Fig. 3: NanoSIMS ^{28}Si ion maps of C. cubana and SBC biofilms. Total ion counts for ^{28}Si were 2.8 times higher in SBC biofilms.

Fig. 4: SEM images and corresponding EDS spectra of SBC biofilms incubated in ASW with 90 ppm silica maintained at pH <7.5 (a) and pH >7.5 (b). The intensities of magnesium and silicon peaks are higher in biofilms incubated at higher pH. These biofilms contained larger colloidal silica particles and grainier texture.

Fig. 5: FTIR spectra of SBC EPS incubated in ASW with 90 ppm silica at pH 6.8 and at pH 8.8. Sulfate groups were present and amorphous silica precipitated in the EPS under both pH conditions.

Fig. 6: Petrographic and SEM images and EDS chemical maps of representative fossiliferous regions of chert from Balbirini Dolomite (thin section 106A; Oehler, 1978). Petrographic images and EDS chemical maps were not collected from identical regions but are from the same laterally continuous microbial lamina in the thin section and are comparable

chemically and mineralogically. Fossiliferous (arrows) and organic rich microbial lamination is present throughout the silicified regions. Silicon/calcium contacts are sharp along the chert/dolomite boundaries. Magnesium is present in both the dolomite and chert.

Fig. 7: Cartoon depiction of a coccoidal cyanobacterial cell surrounded by an EPS envelope containing sulfate and carboxyl functional groups. The cartoon shows negatively charged silicic acid in solution which are then bound to the EPS through cation bridging with magnesium from the surrounding seawater.

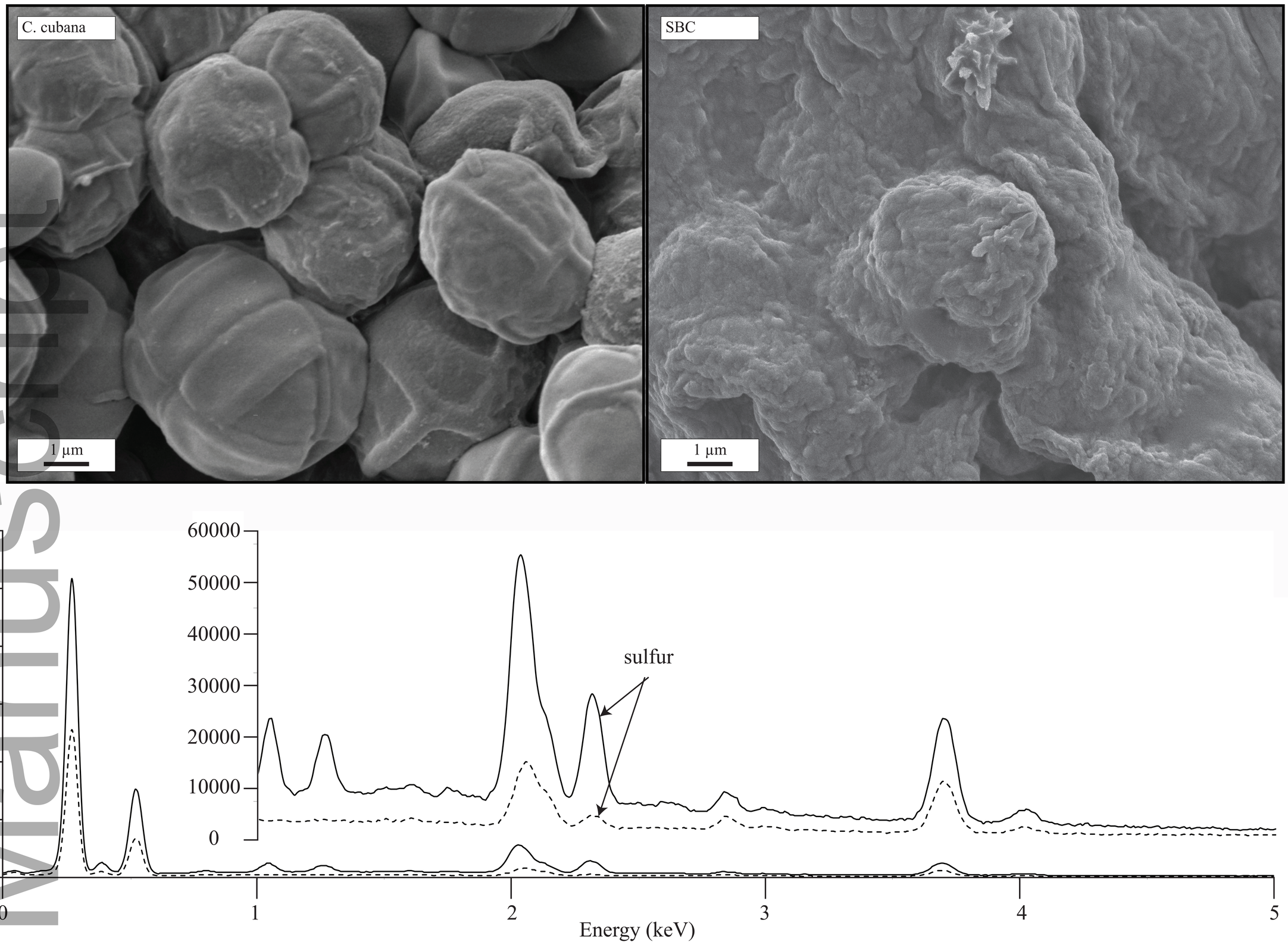

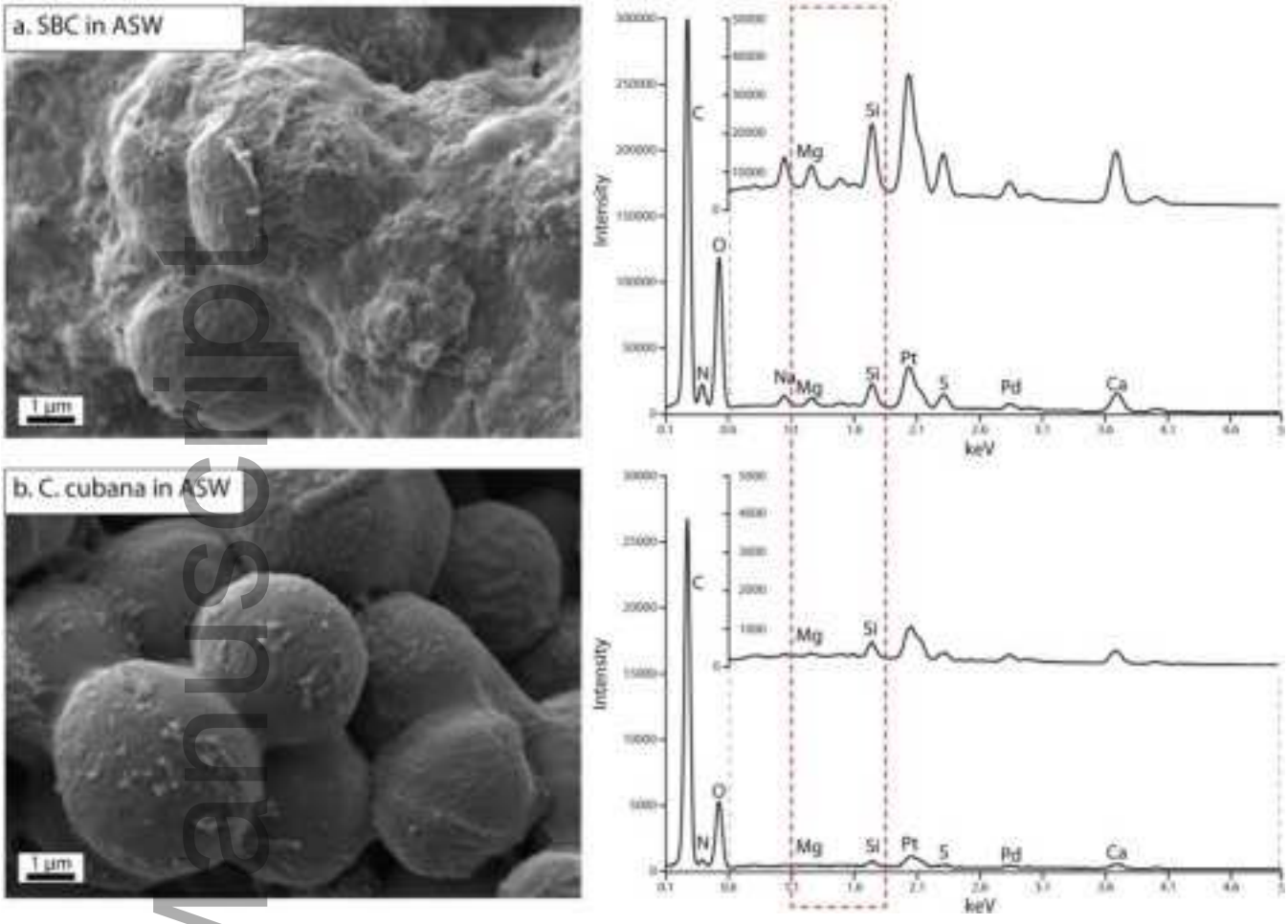

gbi_12447_f2.jpg

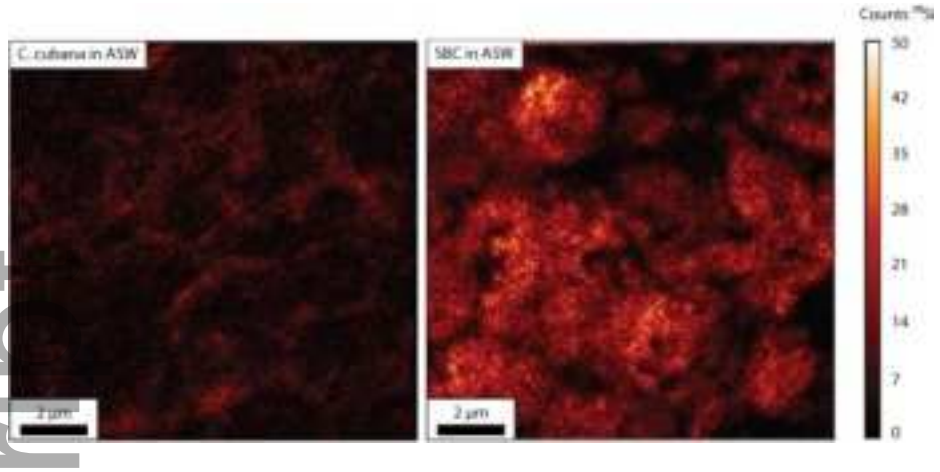

gbi_12447_f3.jpg

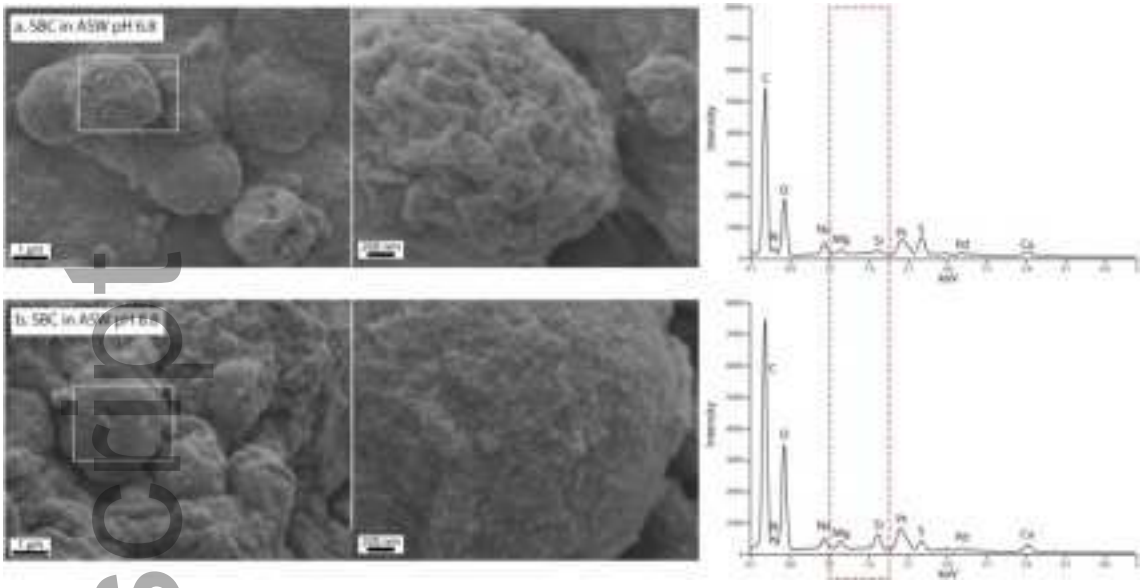

gbi_12447_f4.jpg

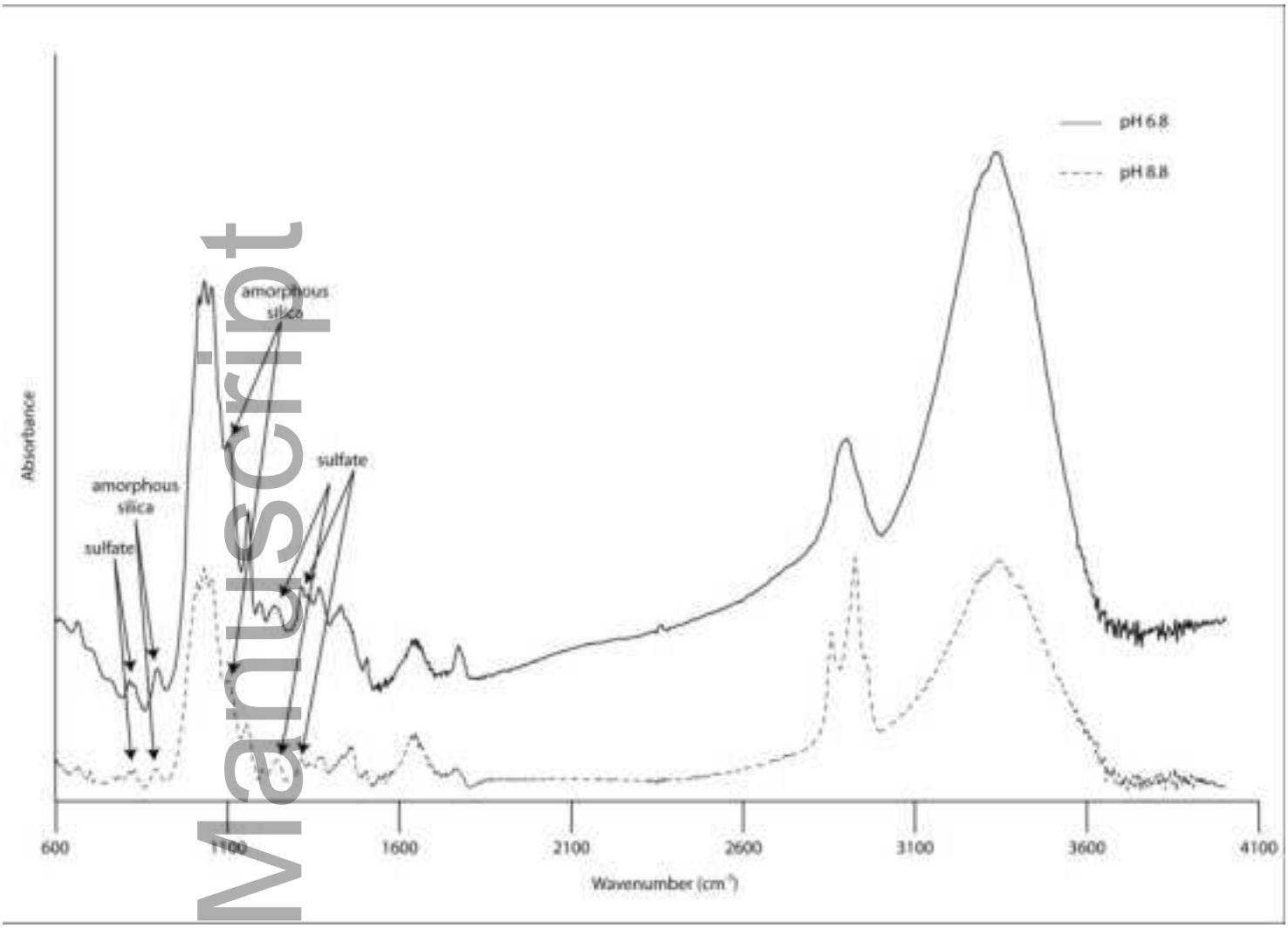

gbi_12447_f5.jpg

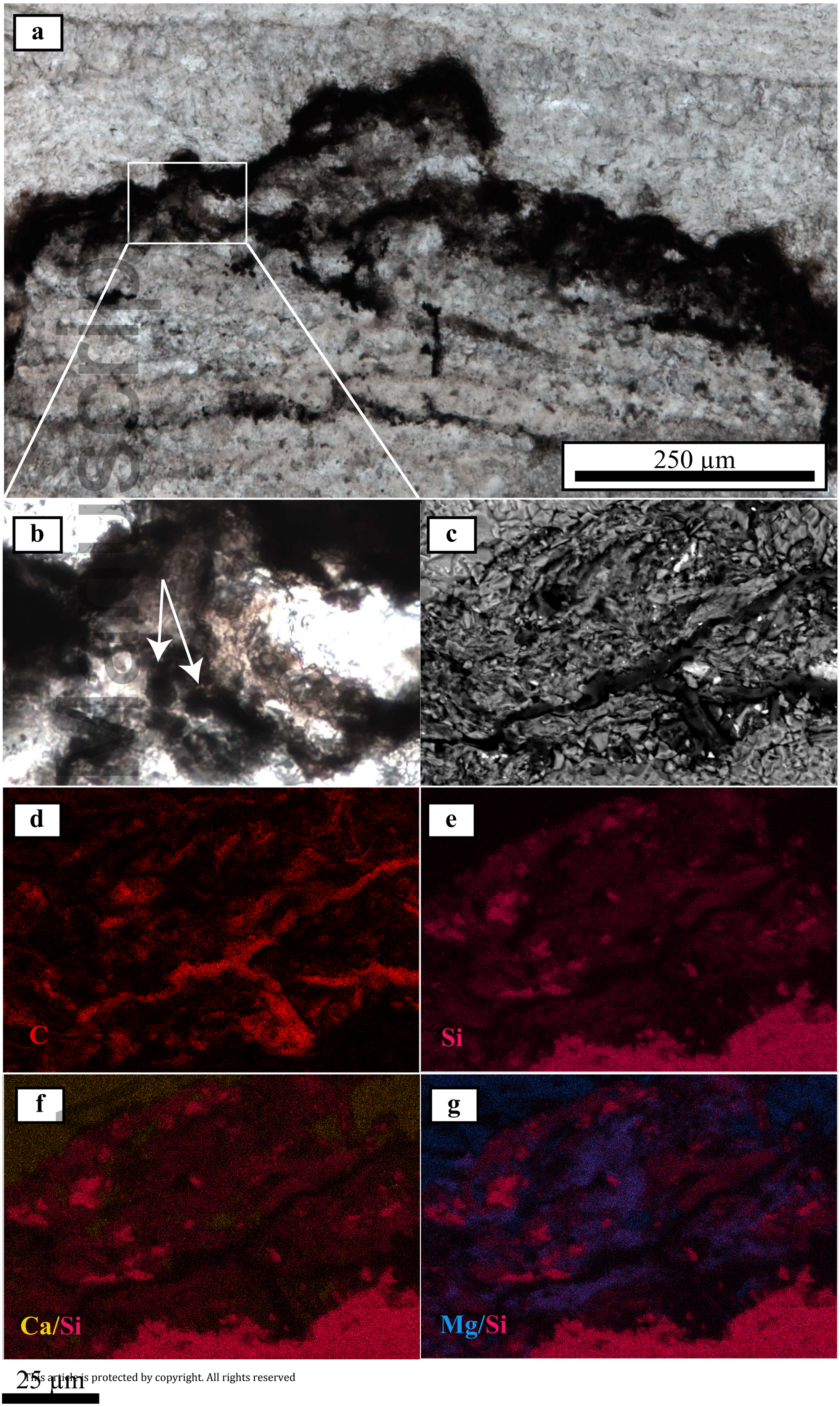

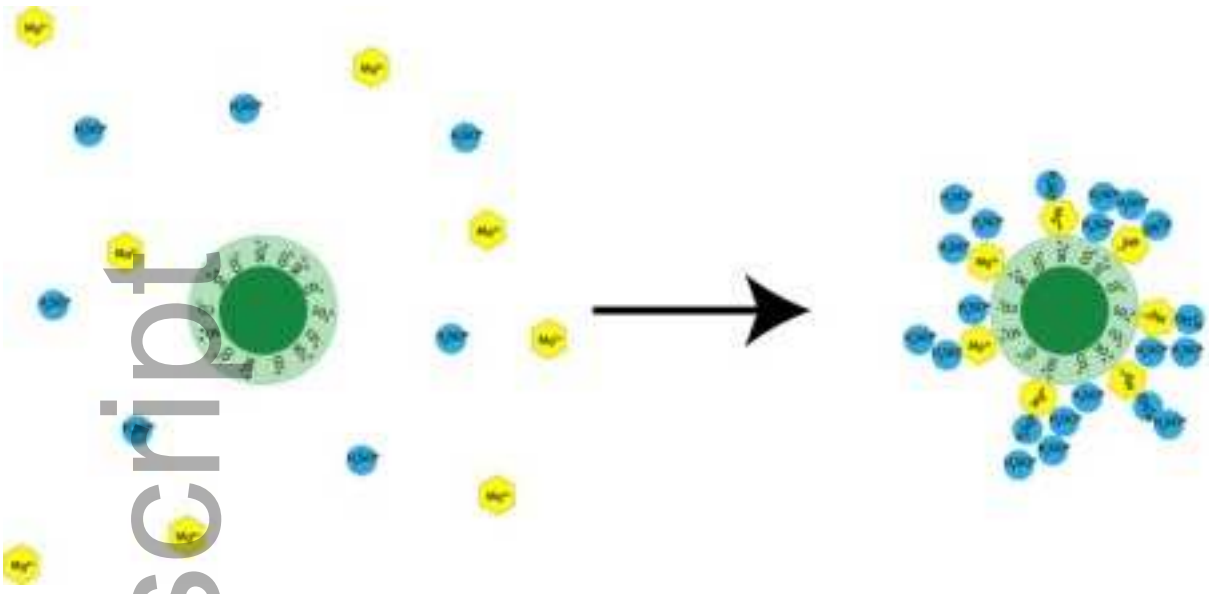

gbi_12447_f7.jpg